Letter

Coherent dynamics of Floquet-Bloch states in monolayer WS_2 reveals fast adiabatic switching

S. K. Earl,[1,2] M. A. Conway,[1,2] J. B. Muir,[1,2] M. Wurdack,[3] E. A. Ostrovskaya,[3] J. O. Tollerud,[1,2] and J. A. Davis[1,2,*]

[1]*Optical Sciences Centre, Swinburne University of Technology, Victoria 3122, Australia*

[2]*ARC Centre of Excellence in Future Low-Energy Electronics Technologies, Swinburne University of Technology, Victoria 3122, Australia*

[3]*ARC Centre of Excellence in Future Low-Energy Electronics Technologies and Nonlinear Physics Centre, Research School of Physics, The Australian National University, Canberra, ACT 2601, Australia*

(Received 13 May 2021; revised 27 July 2021; accepted 28 July 2021; published 12 August 2021)

Floquet engineering offers a path to optically controlled materials, but experimental implementations have frequently relied on femtosecond pulses to achieve the high peak fields required to maximize light-matter interactions and obtain a measurable response. The Floquet formalism, however, is based on a continuous, periodic drive. Here we use femtosecond laser pulses to drive the optical Stark effect, a simple realization of Floquet engineering, in monolayer WS_2. By monitoring the coherent evolution of the free-induction decay, we show that the system evolves adiabatically, and that the finite duration of the pulses does not introduce any effects beyond Floquet theory. Furthermore, we demonstrate that the induced energy shift follows a linear dependence on instantaneous intensity, even for ultrafast driving fields of fewer than 15 optical cycles.

DOI: 10.1103/PhysRevB.104.L060303

Nonequilibrium phases of matter can provide access to microscopic physics, and macroscopic properties, unavailable in extant materials [1–5]. Explorations of materials driven out of equilibrium have led to the discovery of a range of phenomena such as a light-driven anomalous Hall effect [6,7], light-induced superconductivity [8,9], and light-induced phase transitions [10,11]. Floquet engineering [12], the process of using a periodic perturbation to reversibly manipulate band structure, is one avenue to control material properties. Floquet theory removes the time dependence of a Hamiltonian, resulting in an infinite, periodic set of replica bands spaced by the frequency of the perturbation, known as Floquet sidebands [13]. The electromagnetic field oscillations of light can act as the periodic perturbation while careful selection of the energy and other properties can be used to manipulate interactions between the equilibrium bands and their Floquet replicas to control the resulting nonequilibrium properties. Floquet-Bloch bands generated in this manner have been observed, for example, as replicas of the surface states of a topological insulator in time- and angle-resolved photoemission spectroscopy measurements [13,14].

The application of Floquet theory to both the Haldane model [15] and HgTe/CdTe quantum wells [16] predicted a reversible change in the topology of the band structure in both cases. Cold atom experiments have been used to simulate these predictions, showing changes to the topological phase via the Chern number [17,18], and the emergence of chiral edge states [19]. Additionally, experiments with graphene and a circularly polarized mid-IR driving field appear to show the realization of a topologically nontrivial band structure and the opening of a gap, as evidenced by an anomalous Hall effect [6,7,20]. A topological phase transition is also predicted to arise in semiconducting monolayer transition metal dichalcogenides (TMDs) when driven with an optical field with frequency larger than the band gap [21,22], but this is yet to be observed experimentally.

In order to elicit a response in solid-state materials at a detectable level, ultrafast laser pulses with high peak intensities are commonly used because the interactions between states typically scale with the driving field intensity. Floquet theory, however, is predicated on a continuous, monochromatic drive [12,16]. The discrete nature of these pulses then raises new questions: How short can pulses be before Floquet theory ceases to be applicable? When does the band structure (i.e., the eigenstates of the system) cease to evolve adiabatically? The first of these questions was partially addressed using a Green's function analysis that found that the width of the Gaussian envelope was the best predictor of convergence to the case of a continuous drive [23], and Floquet analysis applied to the turning on of a pulse showed a similar result [24]. Experimental measurements in cold atom systems partially addressed this question by comparing the dynamics of a periodically driven system to that of an undriven system with an equivalent Hamiltonian, as a function of the time to ramp on the periodic drive [25]. It was found that even for ramp times as short as half a cycle of the 7.25-kHz drive, the evolution of the driven system matched that of the equivalent undriven one, indicating an adiabatic switching on of the Floquet states, although in that case the periodic drive then remained on for many cycles. In solid-state systems, the inherent timescales are much faster; for example, experiments investigating the optical Stark effect in GaAs quantum wells/bulk GaAs at low temperature found that the adiabatic approximation holds for pulses >100 fs [26–28], corresponding to >40 optical cycles. In this work we go further and test of the suitability of the Floquet picture for pulses as short as 34 fs (<15 optical cycles).

The optical Stark effect (equivalently, the AC Stark effect) is a well-understood phenomenon [29] that emerges naturally

*jdavis@swin.edu.au

from Floquet theory [30]. While it can be derived from the optical Bloch equations for a two-level system within the rotating-wave approximation, we consider it here within the Floquet formalism as an ideal model to test the limits of Floquet theory. The full Floquet Hamiltonian and its properties were discussed by Sie *et al.* [22], yielding a spectral shift, ΔE, given by $\Delta E = M_{ab}^2 \langle \varepsilon^2 \rangle / \Delta$, as expected for the optical Stark shift, where M_{ab} is the polarization matrix element between states $|a\rangle$ and $|b\rangle$, $\langle \varepsilon^2 \rangle$ is the time-averaged value of the electric field squared, and $\Delta = (E_b - E_a) - h\nu$ represents the detuning of the perturbing pulse from the transition. Here we consider the suitability of this approach for short pulses and the adiabaticity of turning on the periodic driving field on femtosecond timescales. In TMD monolayers [21,22,31–34], a valley-selective optical Stark shift has been observed, with the magnitude of the shift obeying the expected linear dependence on pump intensity, and inverse dependence on the detuning of the pump from the transition energy [22,35]. Coherence between valleys was shown to be maintained to some extent, though not quantified, and the phase rotated by the shift [31]. However, little consideration has been given to the duration of the driving field, with the majority of these measurements using pulses longer than 100 fs.

Here, we drive the optical Stark effect in monolayer WS_2 with red-detuned pump pulses as short as 34 fs (∼15 optical cycles) and probe the response with 25 fs pulses, resonant with the exciton transition. By varying the pump-pulse duration while maintaining constant pulse energy, we show that the observed shift scales linearly with peak intensity, as predicted by Floquet theory, and, more significantly, follows (within our time resolution) the instantaneous intensity of the pulse envelope, showing no deviation from Floquet theory and the adiabatic approximation. Furthermore, we observe coherent dynamics of the free-induction decay, revealing a dephasing time of 38.8 fs at room temperature and an adiabatic shift of the transition energy induced by the pump pulse, as identified by the smooth and continuous evolution of the macroscopic coherence through the dynamic shift.

Monolayer WS_2 has a direct gap at the *K*/*K'* symmetry points in the Brillouin zone, and a large exciton binding energy, ∼320 meV [36]. Due to its two constituent elements and hexagonal lattice the crystal structure lacks inversion symmetry, which introduces significant Berry curvature around the *K*/*K'* valleys. Spin-orbit coupling splits the valence and conduction bands, which leads to a spin-valley locking of opposite sign. Consequently, circularly polarized light selectively excites one of the two energetically degenerate valleys, enabling so-called valleytronic applications [37]. This also leads to an optical Stark effect that is valley selective, when driven by a circularly polarized laser field.

To investigate the effect of ultrashort pulses in driving Floquet-Bloch bands, we characterized the Stark shift in a monolayer of WS_2 on a SiO_2/Si substrate using a 25 fs probe pulse, resonant with the *A*-exciton energy (2.025 eV). The shift was induced by the sub-band-gap (1.850 eV) pump pulse whose duration was varied from 34 to 65 fs by altering the spectral bandwidth. The dynamics associated with the observed shift was determined by varying the delay between the pump and probe pulses. Details are provided in the Supplemental Material [38].

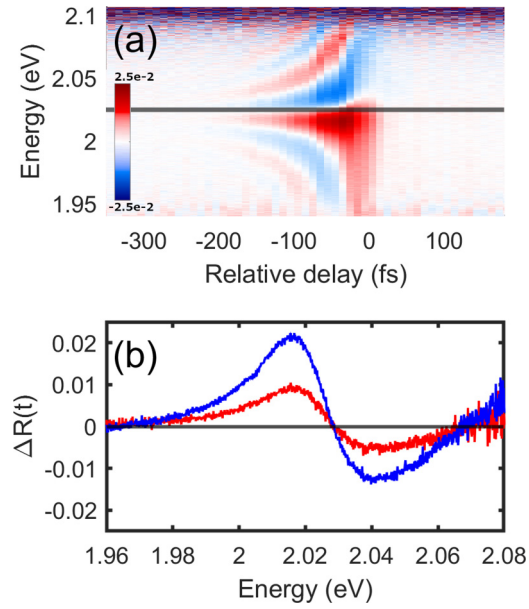

FIG. 1. (a) Measured transient reflectance from 34 fs, 50 $\mu J/cm^2$ pump for cocircularly polarized probe; (b) Maximum signal at pulse overlap (relative delay $t = 0$) for 20 $\mu J/cm^2$ (red) and 50 $\mu J/cm^2$ (blue) pump fluence. Probe fluence was 3.5 $\mu J/cm^2$.

The equilibrium optical properties of the exfoliated WS_2 monolayer were characterized by spatially resolved reflectance contrast and photoluminescence measurements performed at room temperature, as reported previously [39] and are shown in Supplemental Material, Fig. S1 [38]. To account for the influence of the intervening 300 nm SiO_2 layer and Si substrate, a four-Lorentzian model was used to extract the equilibrium permittivity of the WS_2 layer using the transfer matrix method. The resulting equilibrium reflectance and absorption spectra, and the complex permittivity of the monolayer, are presented in Fig. S2. This enabled the conversion of the measured transient reflectance data (dR/R) to the transient absorption of the WS_2 monolayer [38].

The transient reflectance measured with cocircularly polarized pump and probe pulses is shown in Fig. 1(a) for a 34 fs pump pulse duration. The spectral response when pump and probe overlap in time ($t = 0$) is highlighted in Fig. 1(b), and shows a positive peak (increased reflectance due to decreased absorption) on the low-energy side of the exciton and a negative peak (decreased reflectance due to increased absorption) on the high-energy side. This dispersive profile arises from the transition being blueshifted, as a result of the pump-induced optical Stark effect, and is consistent with previous observations [21,22]. The magnitude of the observed shift at $t = 0$ is 0.68 meV, as determined by the spectral weight transfer calculated from the transient absorption spectrum [22,28,38].

For relative delays $t > 0$ (i.e., for the pump pulse arriving first) there is no signal beyond the pulse overlap regime, confirming the expectation that the pump pulse is not generating any significant exciton population. Conversely, for relative delays $t < 0$ a response with fringes is observed [see Fig. 1(a)], persisting beyond −100 fs, well beyond the pulse overlap regime. The fringes represent a spectral interferogram arising from the interference between two pulses separated in time:

the residual probe pulse, and a coherent response generated when the driving field (pump beam) is present.

In this case, the probe beam arrives first and excites a coherent superposition between ground and A-exciton states. This leads to a macroscopic polarization in the monolayer that remains in phase with the initial laser pulse for a time limited by decoherence (due to the finite homogeneous linewidth) and dephasing (due to the finite inhomogeneous linewidth). This macroscopic coherence can reradiate as coherent photoluminescence, in the same direction as the probe, with a π phase shift. This process, also known as free-induction decay, occurs whenever there is coherent resonant excitation. In the absence of the pump this coherent emission adds to the probe, giving the pump-free probe spectrum.

When the driving field is turned on (i.e., when the pump arrives) the energy separation between the ground and A-exciton state increases due to the optical Stark shift. If the eigenstates of the system evolve adiabatically, then the phase of the coherent superposition will evolve smoothly and the macroscopic polarization and the coherent emission will persist, only shifted to this higher energy for the duration of the driving field (pump pulse).

The shift will result in a decrease in the emission at the equilibrium energy and an increase at the blueshifted energy. Because this shifted emission is π out of phase with the incident probe, the net effect of its interference with the probe will be an increase in the measured intensity of the reflected probe on the red side and decrease on the blue side. This is precisely what is seen at pulse overlap ($t = 0$): the spectrally resolved signal gives the dispersive line shape shown in Fig. 1(b). As the delay between the pump and probe increases, the time delay between the shifted coherent emission and the probe with which it interferes also increases, resulting in a spectral interferogram that changes with delay, as shown in Fig. 1(a). To observe this response, the macroscopic polarization must remain coherent, and thus the decay of the response with increasing delay yields a measure of the dephasing of the system.

To confirm that the spectral interference patterns do indeed correspond to a delay between pulses that matches the pump-probe delay, we Fourier transformed the data with respect to the energy (frequency) axis [Fig. 2(a)]. The result shows a signal that does shift in time by an amount equal to the relative delay.

The fringes of the interferogram can be removed by multiplying the complex spectral response by $e^{-i[(\omega-\omega_0)(t+\tau)]}$, which reveals the intrinsic change in reflectance as a function of delay [38]. The dispersive profile, previously only evident at $t = 0$, is now revealed as a function of relative delay between pump and probe in Fig. 2(b). From this, the transient absorption (Fig. S5) can be determined after correcting for substrate reflections and the equilibrium reflectance of the system. The peak of the dispersive feature appears at slightly negative times as it represents the convolution of the pump pulse with the exponential free-induction decay initiated by the arrival of the probe.

Previous work in GaAs/AlGaAs quantum wells observed similar results at low temperature; however, there the coherence times are on the order of picoseconds, and relatively long (200 fs/150 fs) pulses were used [26–28]. The fringes

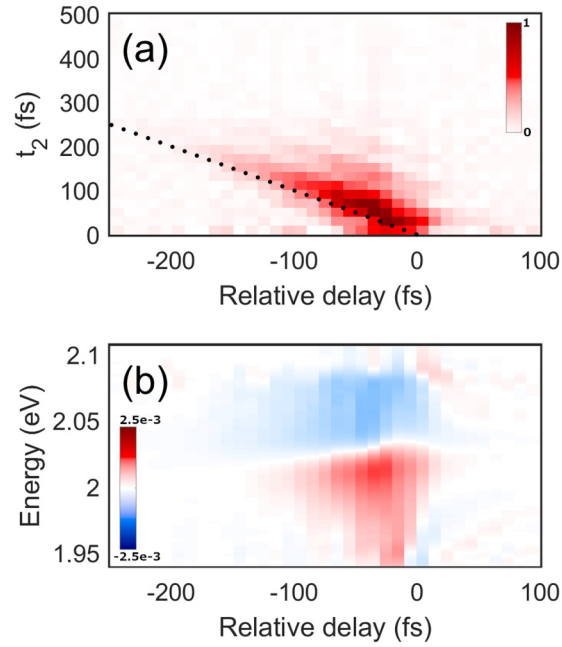

FIG. 2. (a) The Fourier transform of the measured response. The line of slope -1 highlights that the shift in time of the transient feature is equal to the relative delay between pulses. (b) The transient change in reflectance, $\Delta R(t)$, of the WS_2 monolayer after correction for substrate effects.

seen here for $t < 0$ are also similar to what is observed in perturbed free-induction decay, where the free-induction is effectively stopped by the pump pulse. The fringes in that case can arise from nonadiabatic processes and are symmetric about the peak of the absorption. Recent work has reported such symmetric fringes originating from perturbed free-induction decay in an hBN-encapsulated $MoSe_2$ monolayer using degenerate pump-probe spectroscopy [40], where the large pump-induced population of the A exciton (amongst other effects) perturbs the coherent evolution of the free-induction decay. This is in contrast to the observations here, where the fringes are antisymmetric about the equilibrium peak absorption due to the adiabatic spectral shift of the coherent emission.

To confirm the origin of these fringes we performed simple simulations based on the Liouville–von Neumann equation, assuming that the transition energy is adiabatically shifted; that is, the macroscopic coherence is maintained and evolves smoothly as the shift is induced, with the magnitude of the spectral shift following a Gaussian profile matching the pump pulse [38]. Figures 3 and S6 shows the result of these simulations, which qualitatively match the corresponding experimental measurement [Fig. 1(a)]. In contrast, simulations involving either a smooth or rapid reduction of the coherence caused by the pump lead to a symmetric fringe pattern (Fig. S7), which is starkly different from our results. One difference between the experimental and simulation results is the presence of a bending of the nodal line close to $t = 0$. This bending is likely due to additional effects that occur at pulse overlap, which is supported by the observation that as the pump pulse duration increases, the magnitude of the deviation

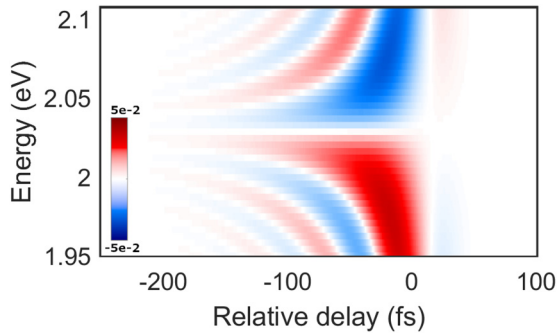

FIG. 3. Simulated pump-probe differential reflectance signal for a 34 fs pump pulse reproduces the dispersive spectral response and fringes at negative delays present in the experimental data in Fig. 1(a).

is reduced and it is stretched over a longer time (see Fig S8). Detailed analysis of these additional effects at pulse overlap is beyond the scope of this work, but may be due to additional reflectance changes arising from the refractive index changes associated with the optical Stark shift, which would only be evident when the probe arrives at the same time as the transition is shifted (i.e., during pulse overlap). Regardless, the clear presence of these antisymmetric fringes for negative delays indicates that the energy of the states changes smoothly, maintaining the macroscopic coherence of the system; i.e., the optical Stark shift is switched on adiabatically.

The dynamics of the Stark shift can in principle then be determined from the calculated transient absorption (Fig. S5). However, the response measured is a convolution of the dynamics of the shift induced by the pump pulse and the probe used to measure it, which includes both the pulse and the resultant free-induction decay. To extract these dynamics, we integrate the absolute value of the Fourier-transformed data in Fig. 2(a), which gives the overall signal response amplitude. Figure 4(a) shows the integrated signal amplitude as a function of delay for the 34 fs pump pulse. It is clear from this plot that at $t < 0$ the signal decays exponentially due to the dephasing, while for positive delays the signal appears to decay with the pulse overlap. This response was fit with an exponential convolved with a Gaussian, where the exponential describes the dephasing of the macroscopic coherence, while the Gaussian part represents the convolution of the probe pulse and the pump-induced Stark shift. From this fit, a value of 38 fs (+4/−3 fs) was obtained for the dephasing time, which is consistent with the linewidth of 32 meV full width at half maximum (FWHM) measured in the linear differential reflectance spectrum with a Gaussian fit to the *A* exciton. To approximate the region of the WS_2 flake sampled by the probe pulse, the linewidth was determined from a spatially averaged region across the flake. It is worth noting that these measures are inclusive of inhomogeneous broadening due to random variations in the dielectric environment [41], and the homogeneous linewidth is likely narrower, as seen in room-temperature coherent four-wave mixing measurements [42]. Still, the observation of a room-temperature dephasing time of >38 fs speaks to the high quality of this exfoliated WS_2 flake (without encapsulation), but also of the potential for

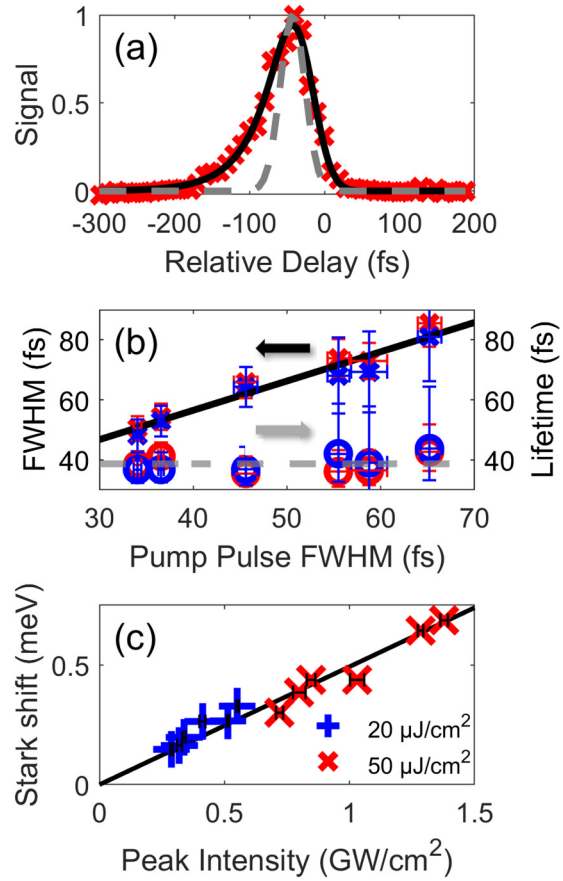

FIG. 4. (a) Integrated response of the absolute value of the Fourier-transformed probe signal (red crosses), with fit line (black). The cross correlation of the pulses (gray dashed line) is aligned to aid comparison; (b) FWHM of the Gaussian component (crosses) and rise time of the exponential component (circles) from the fits for different pulse durations and intensity (red–50 $\mu J/cm^2$; blue–20 $\mu J/cm^2$). A linear fit for the FWHM is included ($y = 0.9762^*x + 17.4564$). (c) Maximum excitonic Stark shift as a function of peak intensity for different pump-pulse durations, together with a linear fit line ($y = 0.4931^*x$; *R* squared = 0.9497).

using these materials in applications where room-temperature coherence is important [43–45].

For positive delays ($t > 0$), the measured response appears to closely follow the pump-pulse envelope. Since the signal amplitude is directly proportional to the magnitude of the Stark shift, this suggests that the shift varies with the instantaneous intensity. To examine this, we repeated these measurements for six different pump pulse durations by reducing the spectral bandwidth, thereby increasing the pump duration from 34 to 65 fs. To maximize time resolution the probe pulse duration was kept at 25 fs. Measurements were collected at fluences of 20 and 50 $\mu J/cm^2$ for both co- and cross-circularly polarized pump and probe. Figures S9 and S10 present the fitted dynamics of all pulses, along with the cross correlation of pump and probe pulses, aligned to facilitate comparison. Figure 4(b) shows the extracted Gaussian FWHM and exponential decay time for all pulses. The exponential decay time stayed constant, regardless of pulse duration or fluence, with a mean value of 39 ± 3 fs. The

Gaussian FWHM, however, increased with the pulse duration, consistent with the convolution of the probe pulse and the Stark shift following the instantaneous intensity of the pump pulse.

Finally, we plot the maximum shift as a function of peak pump intensity for the different pulse durations and energies [Fig. 4(c)]. If there is any nonadiabaticity, deviation from the behavior predicted by Floquet theory, or some delay in the Stark shift turning on, the measured shift would deviate from the expected [21,22] linear trend at short pulse durations. However, for all pulse durations and both fluences, all data points lie on the same linear trend line, further confirming that the magnitude of the Stark shift follows the instantaneous intensity and that these ultrafast pulses drive the optical Stark effect as if the periodic perturbation was a continuous, monochromatic drive.

In conclusion, we have investigated the behavior of the valley-selective optical Stark effect in WS_2 monolayers. By controlling the spectral bandwidth and hence duration and peak intensity of the perturbing pump pulse, we have shown that even for pulses as short as 34 fs (∼15 optical cycles) the optical Stark effect remains proportional to $|\mathbf{E}|$ [2], and follows the instantaneous intensity. More significantly, the observed coherent interference provides strong evidence that the bands of the WS_2 monolayer are adiabatically shifted by the pump. This shift closely follows the envelope of the perturbing pulse, implying an instantaneous response. Together, these findings provide compelling evidence that despite the broad spectral bandwidth and short duration of the pump pulse, the sample responds instantaneously while retaining its macroscopic coherence. It is apparent that the limits of Floquet theory lie at even shorter pulse durations and/or higher intensities. While these experiments were performed in monolayer WS_2, the demonstrated applicability of the Floquet framework to few-cycle pulses should extend to any material system. In particular, where Floquet-Bloch states evolve from the equilibrium states through a quantum phase transition (e.g., the proposed Floquet topological insulator [16]), our results suggest that any nonadiabatic behavior or dynamics beyond the driving pulse envelope can be attributed to the phase transition, because the intrinsic formation of Floquet-Bloch states is essentially instantaneous and adiabatic.

This work was funded by the Australian Research Council Centre of Excellence for Future Low-Energy Electronics Technologies (Grant No. CE170100039). S.K.E. would like to acknowledge Edbert Sie for helpful discussions in relation to the conversion of transient reflectance spectra to transient absorption.

[1] M. Först, C. Manzoni, S. Kaiser, Y. Tomioka, Y. Tokura, R. Merlin, and A. Cavalleri, Nonlinear phononics as an ultrafast route to lattice control, Nat. Phys. **7**, 854 (2011).

[2] S. Kaiser, C. R. Hunt, D. Nicoletti, W. Hu, I. Gierz, H. Y. Liu, M. Le Tacon, T. Loew, D. Haug, B. Keimer, and A. Cavalleri, Optically induced coherent transport far above Tc in underdoped $YBa_2Cu_3O_6+\hat{I}$, Phys. Rev. B **89**, 184516 (2014).

[3] L. Stojchevska, I. Vaskivskyi, T. Mertelj, P. Kusar, D. Svetin, S. Brazovskii, and D. Mihailovic, Ultrafast switching to a stable hidden quantum state in an electronic crystal, Science **344**, 177 (2014).

[4] R. V. Mikhaylovskiy, E. Hendry, A. Secchi, J. H. Mentink, M. Eckstein, A. Wu, R. V. Pisarev, V. V. Kruglyak, M. I. Katsnelson, Th. Rasing, and A. V. Kimel, Ultrafast optical modification of exchange interactions in iron oxides, Nat. Commun. **6**, 8190 (2015).

[5] M. Mitrano, A. Cantaluppi, D. Nicoletti, S. Kaiser, A. Perucchi, S. Lupi, P. Di Pietro, D. Pontiroli, M. Riccò, S. R. Clark, D. Jaksch, and A. Cavalleri, Possible light-induced superconductivity in K_3C_{60} at high temperature, Nature (London) **530**, 461 (2016).

[6] J. W. McIver, B. Schulte, F. U. Stein, T. Matsuyama, G. Jotzu, G. Meier, and A. Cavalleri, Light-induced anomalous Hall effect in graphene, Nat. Phys. **16**, 38 (2020).

[7] S. A. Sato, J. W. McIver, M. Nuske, P. Tang, G. Jotzu, B. Schulte, H. Hübener, U. De Giocannini, L. Mathey, M. A. Sentef, A. Cavalleri, and A. Rubio, Microscopic theory for the light-induced anomalous Hall effect in graphene, Phys. Rev. B **99**, 214302 (2019).

[8] D. Fausti, R. I. Tobey, N. Dean, S. Kaiser, A. Dienst, M. C. Hoffmann, S. Pyon, T. Takayama, H. Takagi, and A. Cavalleri, Light-induced superconductivity in a stripe-ordered cuprate, Science **331**, 189 (2011).

[9] E. Snider, N. Dasenbrock-Gammon, R. McBride, M. Debessi, H. Vindana, K. Vencatasamy, K. V. Lawler, A. Salamat, and R. P. Dias, Room-temperature superconductivity in a carbonaceous sulfur hydride, Nature (London) **586**, 373 (2020).

[10] M. Fiebig, K. Miyano, Y. Tokura, and Y. Tomioka, Visualization of the local insulator-metal transition in $Pr_{0.7}Ca_{0.3}MnO_3$, Science **280**, 1925 (1998).

[11] A. Cavalleri, C. s. Tóth, C. W. Siders, J. A. Squier, F. Ráksi, P. Forget, and J. C. Kieffer, Femtosecond Structural Dynamics in VO_2 during an Ultrafast Solid-Solid Phase Transition, Phys. Rev. Lett. **87**, 237401 (2001).

[12] J. H. Shirley, Solution of the Schrödinger equation with a Hamiltonian periodic in time, Phys. Rev. **138**, B979 (1965).

[13] Y. H. Wang, H. Steinberg, P. Jarillo-Herrero, and N. Gedik, Observation of Floquet-Bloch states on the surface of a topological insulator, Science **342**, 453 (2013).

[14] F. Mahmood, C.-K. Chan, Z. Alpichshev, D. Gardner, Y. Lee, P. A. Lee, and N. Gedik, Selective scattering between Floquet-Bloch and Volkov states in a topological insulator, Nat. Phys. **12**, 306 (2016).

[15] J.-I. Inoue and A. Tanaka, Photoinduced Transition between Conventional and Topological Insulators in Two-Dimensional Electronic Systems, Phys. Rev. Lett. **105**, 017401 (2010).

[16] N. H. Lindner, G. Refael, and V. Galitski, Floquet topological insulator in semiconductor quantum wells, Nat. Phys. **7**, 490 (2011).

[17] M. Aidelsburger, M. Lohse, C. Schweizer, M. Atala, J. T. Barreiro, S. Nascimbène, N. R. Cooper, I. Bloch, and

N. Goldman, Measuring the Chern number of Hofstadter bands with ultracold bosonic atoms, Nat. Phys. **11**, 162 (2015).

[18] G. Jotzu, M. Messer, R. Desbuquois, M. Lebrat, T. Uehlinger, D. Greif, and T. Esslinger, Experimental realization of the topological Haldane model with ultracold fermions, Nature (London) **515**, 237 (2014).

[19] M. Mancini, G. Pagano, G. Cappellini, L. Livi, M. Rider, J. Catani, C. Sias, P. Zoller, M. Inguscio, M. Dalmonte, and L. Fallani, Observation of chiral edge states with neutral fermions in synthetic Hall ribbons, Science **349**, 1510 (2015).

[20] T. Oka and H. Aoki, Photovoltaic Hall effect in graphene, Phys. Rev. B **79**, 081406(R) (2009).

[21] J. Kim, X. Hong, C. Jin, S.-F. Shi, C.-Y. S. Chang, M.-H. Chiu, L.-J. Li, and F. Wang, Ultrafast generation of pseudo-magnetic field for valley excitons in WSe_2 monolayers, Science **346**, 1205 (2014).

[22] E. J. Sie, J. W. McIver, Y.-H. Lee, L. Fu, J. Kong, and N. Gedik, Valley-selective optical Stark effect in monolayer WS_2, Nat. Mater. **14**, 290 (2015).

[23] M. H. Kalthoff, G. S. Uhrig, and J. K. Freericks, Emergence of Floquet behavior for lattice fermions driven by light pulses, Phys. Rev. B **98**, 035138 (2018).

[24] U. De Giovannini and H. Huebener, Floquet analysis of excitations in materials, J. Phys. Mater. **3**, 012001 (2020).

[25] M. Messer, K. Sandholzer, F. Görg, J. Minguzzi, R. Desbuquois, and T. Esslinger, Floquet Dynamics in Driven Fermi-Hubbard Systems, Phys. Rev. Lett. **121**, 233603 (2018).

[26] M. Joffre, D. Hulin, J.-P. Foing, J.-P. Chambaret, A. Migus, and A. Antonetti, Dynamics and Fourier transform studies of the excitonic optical Stark effect, IEEE J. Quantum Electron. **25**, 2505 (1989).

[27] M. Joffre, D. Hulin, A. Migus, and A. Antonetti, Dynamics of the optical Stark effect in semiconductors, J. Mod. Opt. **35**, 1951 (1988).

[28] M. Joffre, D. Hulin, A. Migus, A. Antonetti, C. Benoit à la Guillaume, N. Peychambarian, M. Lindberg, and S. W. Koch, Coherent effects in pump-probe spectroscopy of excitons, Opt. Lett. **13**, 276 (1988).

[29] S. H. Autler and C. H. Townes, Stark effect in rapidly varying fields, Phys. Rev. **100**, 703 (1955).

[30] U. De Giovannini, H. Hübener, and A. Rubio, Monitoring electron-photon dressing in WSe_2, Nano Lett. **16**, 7993 (2016).

[31] Z. Ye, D. Sun, and T. F. Heinz, Optical manipulation of valley pseudospin, Nat. Phys. **13**, 26 (2017).

[32] C. Yong, J. Horng, Y. Shen, H. Cai, A. Wang, C.-S. Yang, C.-K. Lin, S. Zhao, K. Watanabe, T. Taniguchi, S. Tongay, and F. Wang, Biexcitonic optical Stark effects in monolayer molybdenum diselenide, Nat. Phys. **14**, 1092 (2018).

[33] P. D. Cunningham, A. T. Hanbicki, T. L. Reinecke, K. M. McCreary, and B. T. Jonker, Resonant optical Stark effect in monolayer WS_2, Nat. Commun. **10**, 5539 (2019).

[34] D. J. Morrow, D. D. Kohler, Y. Zhao, J. M. Scheeler, S. Jin, and J. C. Wright, Quantum interference between the optical Stark effect and resonant harmonic generation in WS_2, Phys. Rev. B **102**, 161401(R) (2020).

[35] M. Combescot and R. Combescot, Excitonic Stark shift: A Coupling to 'Semivirtual" biexcitons, Phys. Rev. Lett. **61**, 117 (1988).

[36] A. Chernikov, T. C. Berkelbach, H. M. Hill, A. Rigosi, Y. Li, O. B. Aslan, D. R. Reichman, M. S. Hybertson, and T. F. Heinz, Exciton Binding Energy and Nonhydrogenic Rydberg Series in Monolayer WS_2, Phys. Rev. Lett. **113**, 076802 (2014).

[37] K. F. Mak, K. He, J. Shan, and T. F. Heinz, Control of valley polarization in monolayer MoS_2 by optical helicity, Nat. Nanotechnol. **7**, 494 (2012).

[38] See Supplemental Material at http://link.aps.org/supplemental/10.1103/PhysRevB.104.L060303 for methods, sample details, and equilibrium properties, details of the analyses and simulations discussed in the main text and the full set of raw experimental measurements, which includes Refs. [46–53].

[39] P. V. Kolesnichenko, Q. Zhang, T. Yun, C. Zheng, M. S. Fuhrer, and J. A. Davis, Disentangling the effects of doping, strain and disorder in monolayer WS_2 by optical spectroscopy, 2D Mater. **7**, 025008 (2020).

[40] A. Rodek, T. Hahn, J. Kasprzak, T. Kazimierczuk, K. Nogajewski, K. Połczyńska, K. Watanabe, T. Taniguchi, T. Kuhn, P. Machnikowski, M. Potemski, D. Wigger, and P. Kossacki, Exciton dynamics in hBN/$MoSe_2$/hBN heterostructures measured in pump-probe spectroscopy, arXiv:2103.05328 [cond-mat.mes-hall].

[41] L. W. Raja, L. Zipfel, Y. Cho, S. Brem, A. D. Ziegler, M. Kulig, T. Taniguchi, K. Watanabe, E. Malic, T. F. Heinz, T. C. Berkelbach, and A. Chernikov, Dielectric disorder in two-dimensional materials, Nat. Nanotechnol. **14**, 832 (2019).

[42] M. Wurdack, E. Estrecho, S. Todd, T. Yun, M. Pieczarka, S. K. Earl, J. A. Davis, C. Schneider, A. G. Truscott, and E. A. Ostrovskaya, Motional narrowing, ballistic transport, and trapping of room-temperature exciton polaritons in an atomically-thin semiconductor, arXiv:2103.11591 [cond-mat.mes-hall].

[43] M. Zamfirescu, A. Kavokin, B. Gil,G. Malpuech, and M. Kaliteevski, ZnO as a material mostly adapted for the realization of room-temperature polariton lasers, Phys. Rev. B **65**, 161205(R) (2002).

[44] S. Christopoulos, G. Baldassarri Höger von Högersthal, A. J. D. Grundy, P. G. Lagoudakis, A. V. Kavokin, J. J. Baumberg, G. Christmann, R. Butté, E. Feltin, J.-F. Carlin, and N. Grandjean, Room-Temperature Polariton Lasing in Semiconductor Microcavities, Phys. Rev. Lett. **98**, 126405 (2007).

[45] F. Novelli, A. Nazir, G. H. Richards, A. Roozbeh, K. E. Wilk, P. M. G. Curmi, and J. A. Davis, Vibronic resonances facilitate excited-state coherence in light-harvesting proteins at room temperature, J. Phys. Chem. Lett. **6**, 4573 (2015).

[46] D. Polli, L. Lüer, and G. Cerullo, High-time-resolution pump-probe system with broadband detection for the study of time-domain vibrational dynamics, Rev. Sci. Instrum. **78**, 103108 (2007).

[47] J. Brazard, L. A. Bizimana, and D. B. Turner, Accurate convergence of transient-absorption spectra using pulsed lasers, Rev. Sci. Instrum. **86**, 053106 (2015).

[48] C. Schriever, S. Lochbrunner, E. Riedle, and D. J. Nesbitt, Ultrasensitive ultraviolet-visible 20 fs absorption spectroscopy of low vapor pressure molecules in the gas phase, Rev. Sci. Instrum. **79**, 013107 (2008).

[49] M. A. Green, Self-consistent optical parameters of intrinsic silicon at 300 K including temperature coefficients, Sol. Energy Mater. Sol. Cells **92**, 1305 (2008).

[50] I. H. Malitson, Interspecimen comparison of the refractive index of fused silica, J. Opt. Soc. Am. **55**, 1205 (1965).

[51] Y. Li, A. Chernikov, X. Zhang, A. Rigosi, H. M. Hill, A. M. van de Zande, D. A. Chenet, E.-M. Shih, J. Hone, and T. F. Heinz, Measurement of the optical dielectric function of monolayer transition-metal dichalcogenides: MoS_2, $MoSe_2$, WS_2, and WSe_2, Phys. Rev. B **90**, 205422 (2014).

[52] E. J. Sie, A. J. Frenzel, Y.-H. Lee, J. Kong, and N. Gedik, Intervalley biexcitons and many-body effects in monolayer MoS_2, Phys. Rev. B **92**, 125417 (2015).

[53] A. B. Kuzmenko, Kramers-Kronig constrained variational analysis of optical spectra, Rev. Sci. Instrum. **76**, 083108 (2005).